Supporting Information

Electrolyte design weakens lithium-ion solvation energy for a fast-charging and long-cycling Si anode

Min Li[a,b], Shuai Li[a], Dong Yan[a], Yuhao Ma[a], Xiaobin Niu[a] and Liping Wang*[a]

[a] *School of Materials and Energy, University of Electronic Science and Technology of China, Chengdu 611731, China*

[b] *Tianmu Lake Institute of Advanced Energy Storage Technologies Institution, Changzhou 213300, China*

* Corresponding authors.

Corresponding author at: School of Materials and Energy, University of Electronic Science and Technology of China, Chengdu 611731, China.

E-mail: lipingwang@uestc.edu.cn (L. Wang).

Experimental Section

4.1 Preparation of electrolytes

Battery-grade LiFSI, solution of FEC, Ethylene carbonate (EC), Dimethyl carbonate (DMC), Diethyl carbonate (DEC), and Ethyl Methyl Carbonate (EMC) were received from Suzhou DoDoChem Technology Co., Lt. LiDFOB additive was purchased from Shanghai Dibo Biotechnology Co., LTD. Ethyl acetate (EA) and ethyl fluoroacetate (EFA) were purchased from Shanghai Aladdin Biochemical Technology Co., Ltd. For EA/FEC-based, and EFA/FEC-based electrolytes, 280.5 mg LiFSI and 14.4 mg LiDFOB were dissolved in 1 mL solvent/FEC mixtures (8:2 by volume). For EC-based electrolyte, 1 mol L^{-1} $LiPF_6$ was dissolved in EC/DMC (1:1, by volume) with 10 wt% FEC. Electrolyte preparation was done in an argon-filled glovebox (oxygen, water content < 0.1 ppm).

4.2 Electrodes preparation

The commercialized micron Si/C sphere was obtained from Physcience Golden Silicon New Material Technology Co., Ltd., Sichuan. Si anodes were fabricated with 80 wt% Si/C sphere, 10 wt% conductive agent (Super P: carbon nanotubes=8:2) and 10 wt% binder (PAA), grinding to obtain a homogeneous slurry using deionized water. The slurry was uniformly cast on commercial Cu foil and dried at 80°C overnight, which was then punched into discs with a diameter of 11 mm. The typical mass loading of the Si/C anode was about 1.0 mg cm^{-2}. The LFP cathodes were fabricated with 80 wt% LFP, 10 wt% super P, and 10 wt% PVDF. The mixture was dispersed in NMP, and the slurry was coated onto Al foil, then it underwent the same process as the anode. The mass loading of the LFP cathode was about 8 mg cm^{-2}.

4.3 Electrochemical Measurements

Li||Si/C half cells and Si/C||LFP full cells were assembled in CR2032-type coin cell configurations, and the Si/C anode was electrochemically pre-lithiated with an N/P ratio of 1.12 before cycling in full cells. The separator was Celgard 2500 (thickness=16 μm, diameter=19 mm), and 50 μL of electrolyte was added for each cell. The cycling and rate performance of the cells was investigated on a Neware battery tester (CT-3008W, Shenzhen, China). The voltage range of the Li/Si cells is 0.01-2 V, and the Si/C||LFP cells were tested at the voltage range of 2.3–3.8 V. The electrochemical impedance spectra (EIS) were obtained by using an electrochemical workstation (CHI660E, Chenhua, Shanghai), and the frequency range of the EIS test is 0.01–10^5 Hz with an AC signal of 5 mV. The Li-ion transfer number (t_{Li^+}) was characterized by the steady state polarization method in Li/Li cells with a polarization voltage of 0.01 V. according to the equation (1):

$$t_{Li^+} = \frac{I_s\left(\Delta V - I_0 R^0\right)}{I_0\left(\Delta V - I_s R^s\right)} \#(1)$$

where I_0 and I_s are initial and steady-state current, which were recorded by chronoamperometry for 3000s. R^0 and R^s are interfacial resistance between the electrode and electrolyte before and after the test. The activation energy of Li^+ desolvation was evaluated by analyzing fitting results of the temperature-dependent EIS, based on the Arrhenius equation:

$$\frac{1}{R_{ct}} = A\, exp\left(\frac{-E_a}{RT}\right) \#(2)$$

where A, E_a, R, and T are frequency factor, activation energy, gas constant, and absolute temperature respectively.

4.4 Characterizations

The cycle cells were completely charged to 2.0 V and disassembled in an argon-filled glove box. Then, the acquired electrode sheets were washed three times with the appropriate electrolyte solvents to remove residual electrolyte and subsequently dried for 24 h. Fourier transform infrared (FT-IR) spectra were collected by Thermo Scientific Nicolet iS50. Raman spectra were collected by Horiba LabRAM HR Evolution with a laser at 532 nm. The surface component of the silicon-carbon anode was acquired by XPS (Thermo Fischer). Transmission Electron Microscope (Tecnai G2 F20 S-Twin TMP) was used to study the SEI films cycled in different electrolytes. The electrode thicknesses cycled in different electrolytes were explored by an optical microscope (Yuescope YM520).

4.5 MD simulation methodology

In this study, molecular models of Li^+, FSI, EA, EFA, FEC, and DFOB were constructed using Materials Studio. Gaussian 16 code was used to optimize the structures of two molecules using the B3LYP-D3 functional and the 6-311G basis set. Other bonds and non-bond parameters were obtained via Sobtop. All-atom MD simulations were conducted using the GROMACS software package, version 2021.5. [1-3] The Amber03 force field[4] was employed to describe the molecule, together with the TIP3P[5] water model.

First, we insert 160 Li^+, 150 FSI, 816 EA, 274 FEC, and 10 DFOB molecules into a cubic box with dimensions 10 nm × 10 nm × 10 nm, and then fill the entire box with water to construct System 1. Then 160 Li^+, 150 FSI, 774 EFA, 274 FEC, and 10 DFOB molecules were randomly inserted into system 2. Initially, both systems underwent energy minimization. Each system was minimized using the steepest descent method to correct the initial contact problem, followed by a short simulation of 500 ps using

the NVT and NPT systems. Subsequently, the position restraints were lifted to conduct a data production run lasting 20 ns with the NPT ensemble. The pressure was maintained at P=1.0 bar using a Berendsen barostat, and the temperature was controlled at 300 K using a velocity-rescale thermostat with a coupling constant of τ=0.1 ps. Nonbonded interactions were computed with a cutoff of 1.2 nm, and long-range electrostatic interactions were computed using the particle-mesh Ewald summation method. All bonds were constrained using the LINCS algorithm.[6] Simulations were performed with a time step of 2 fs, and the neighbor list was updated every 10 steps. Periodic boundary conditions were applied in all three directions. PyMOL-3.0.3 was used for visualization.

The radial distribution function (RDF) and coordination number of Li^+ with other molecules in the two systems were calculated. The radial distribution function, which is the most important function for describing the structural characteristics of the fluid, is defined as shown in equation (3):

$$g_{\alpha\beta}(r) = \frac{1}{4\pi\rho_{\beta}r^2}\left[\frac{dN_{\alpha\beta}(r)}{dr}\right] \#(3)$$

where ρ_{β} is the number density of the β particles, and $N_{\alpha\beta}(r)$ denotes the average number of β particles that are located in a sphere centered on the α particles with r as the radius.

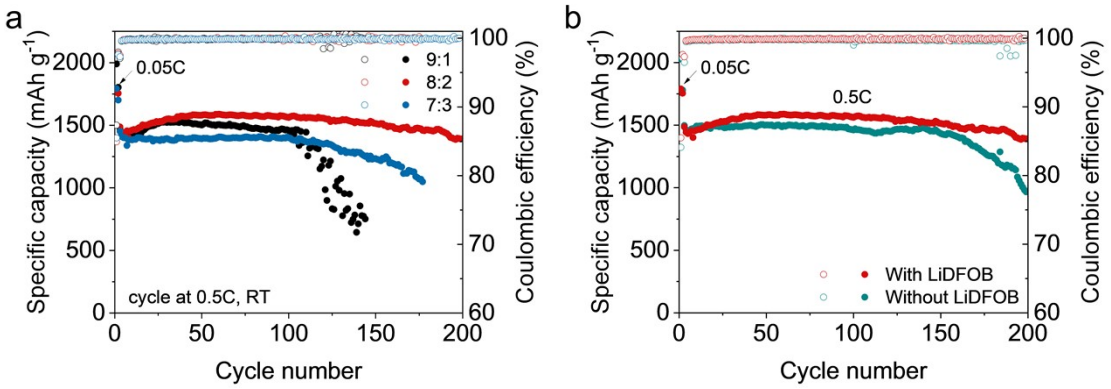

Fig. S1. (a) The cycle performance of Li/Si cells at 0.5C using electrolytes: 1.5 M LiFSI and 0.1 M LiDFOB in EFA/FEC(x:y, by volume). (b) The cycling performance of the cells using EFA/FEC-based electrolytes with and without LiDFOB.

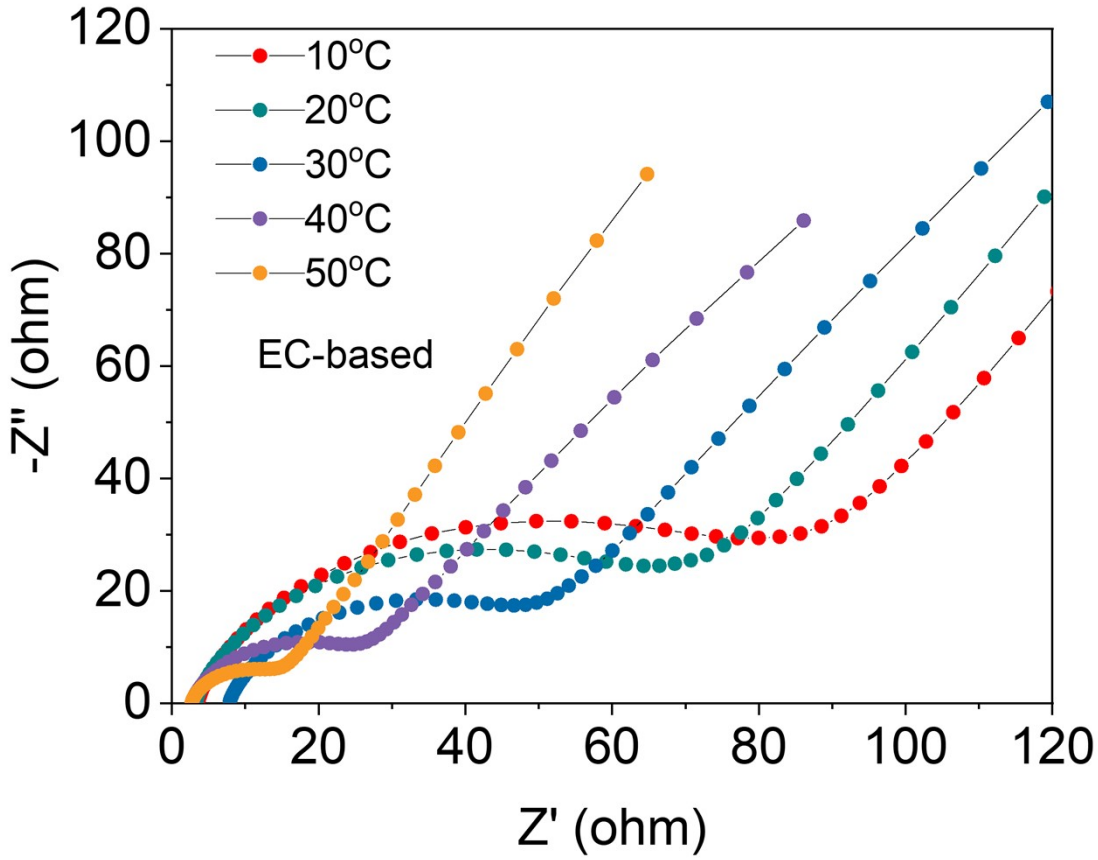

Fig. S2. Nyquist plots of the Si/Si symmetric cells using the EC-based electrolyte at 10°C to 50°C after five formation cycles.

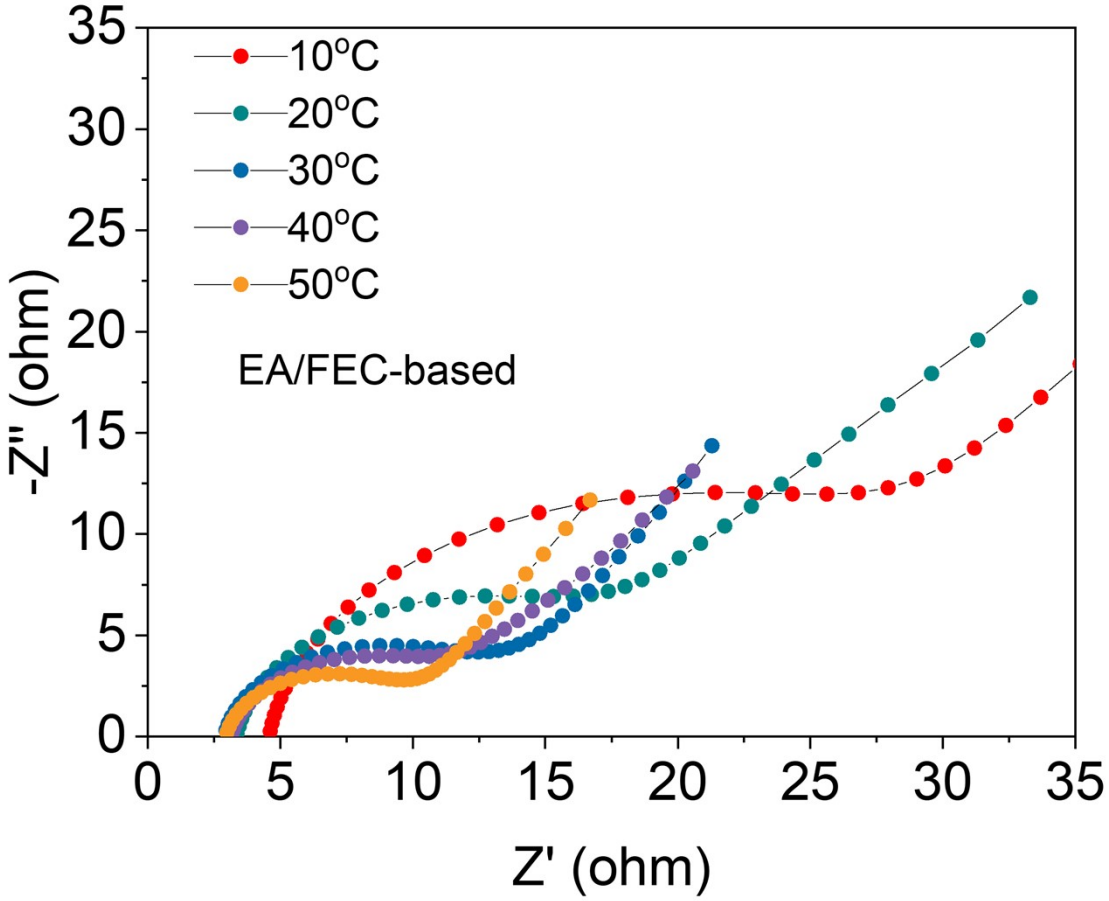

Fig. S3. Nyquist plots of the Si/Si symmetric cells using the EA/FEC-based electrolyte at 10°C to 50°C after five formation cycles.

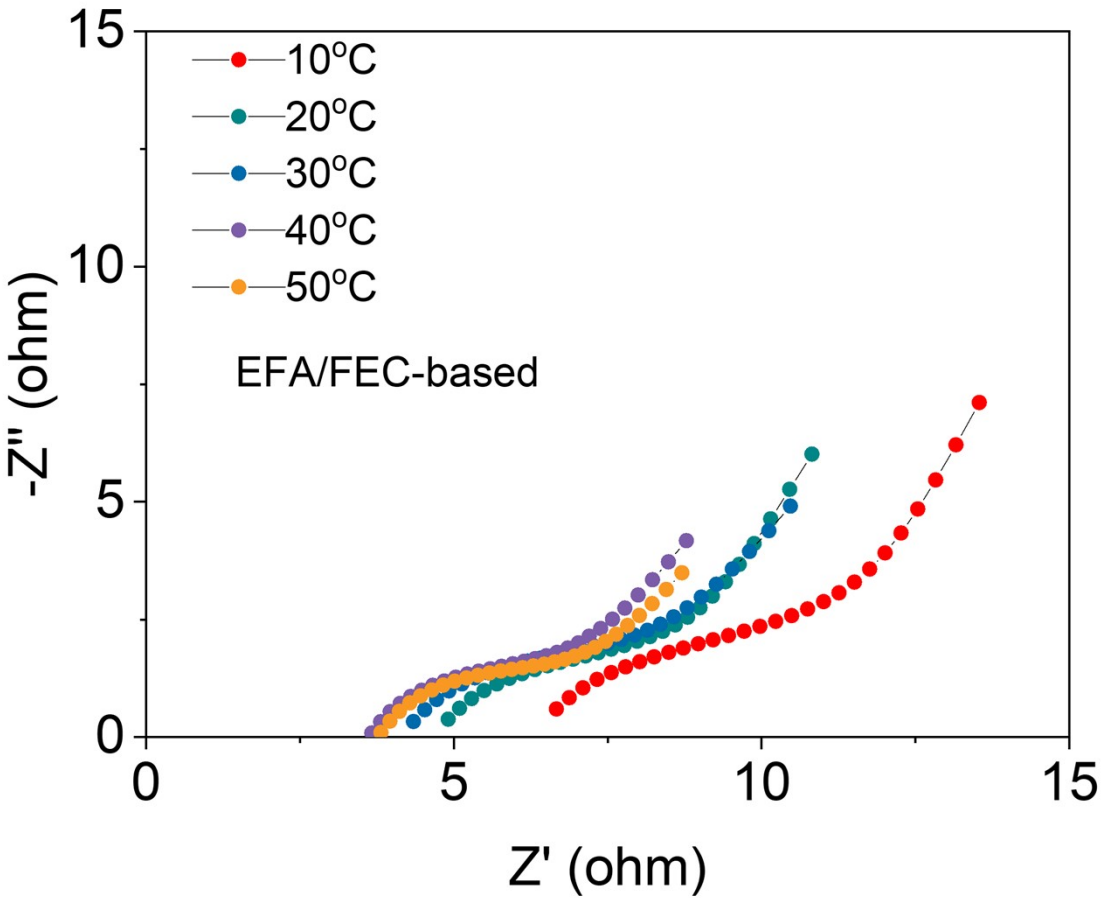

Fig. S4. Nyquist plots of the Si/Si symmetric cells using the EFA/FEC-based electrolyte at 10°C to 50°C after five formation cycles.

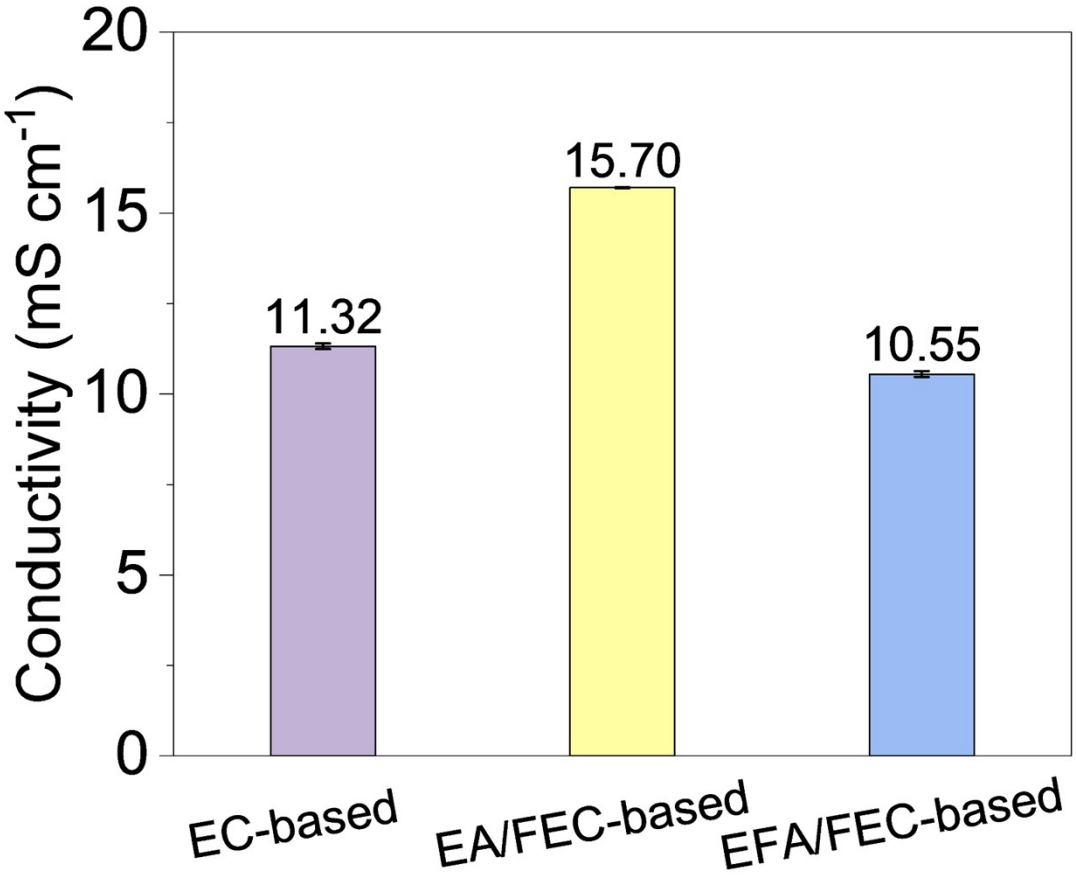

Fig. S5. The ionic conductivity of different electrolytes at RT.

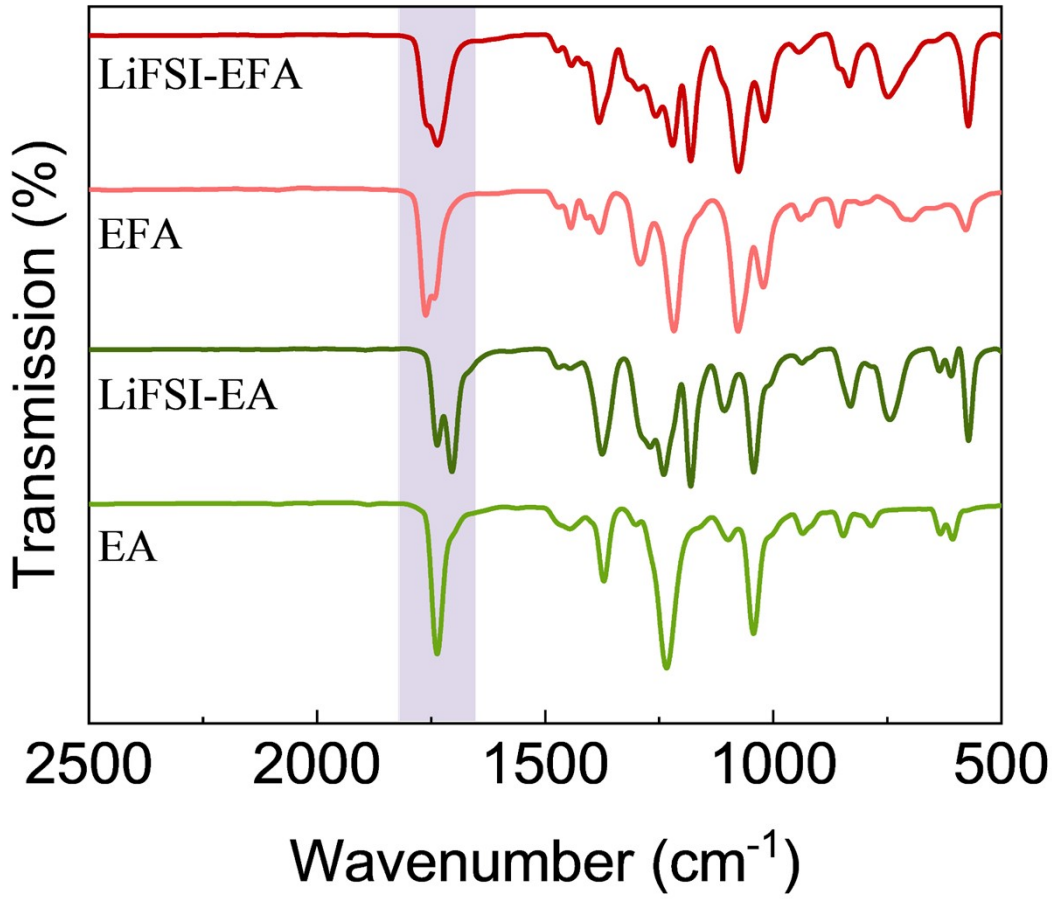

Fig. S6. FTIR spectra of EA solvent, LiFSI-EA (1.5 M LiFSI in EA), EFA solvent, and LiFSI-EFA (1.5 M LiFSI in EFA).

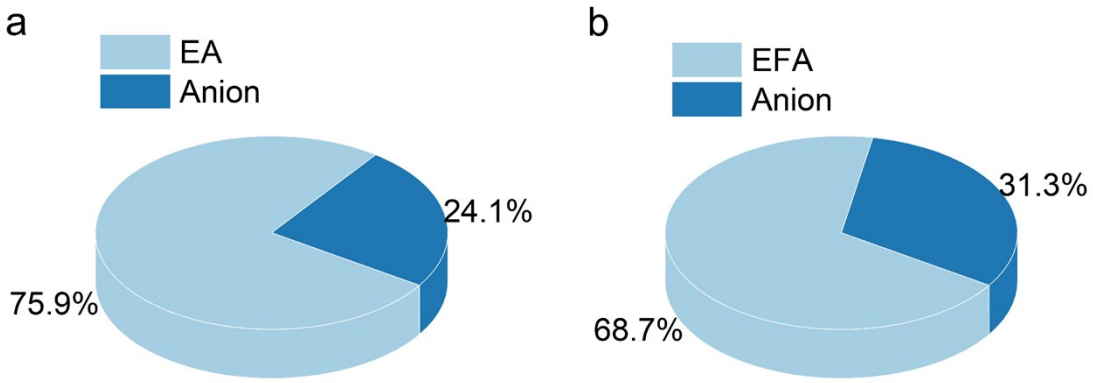

Fig. S7. The proportion of solvents and anions in the Li^+ solvation configuration in (a) EA/FEC-based and (b) EFA/FEC-based electrolytes.

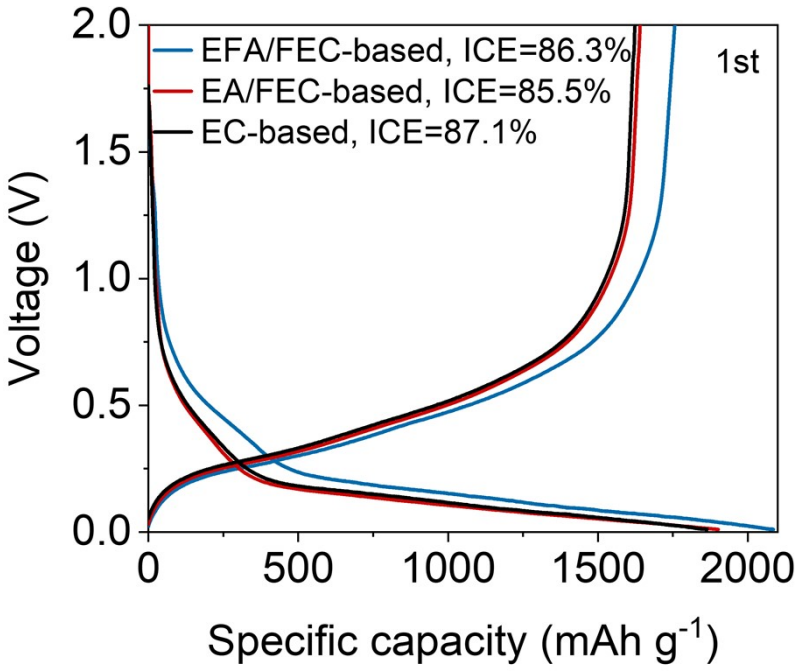

Fig. S8. The first charge/discharge curves of Li/Si cells with different electrolytes at RT.

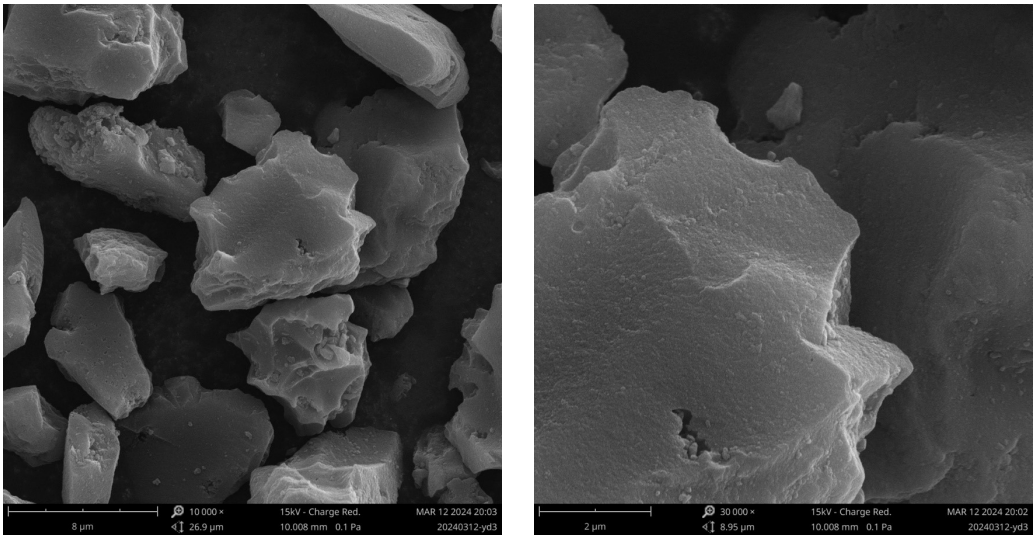

Fig. S9. SEM images of the pristine commercial Si/C anode materials.

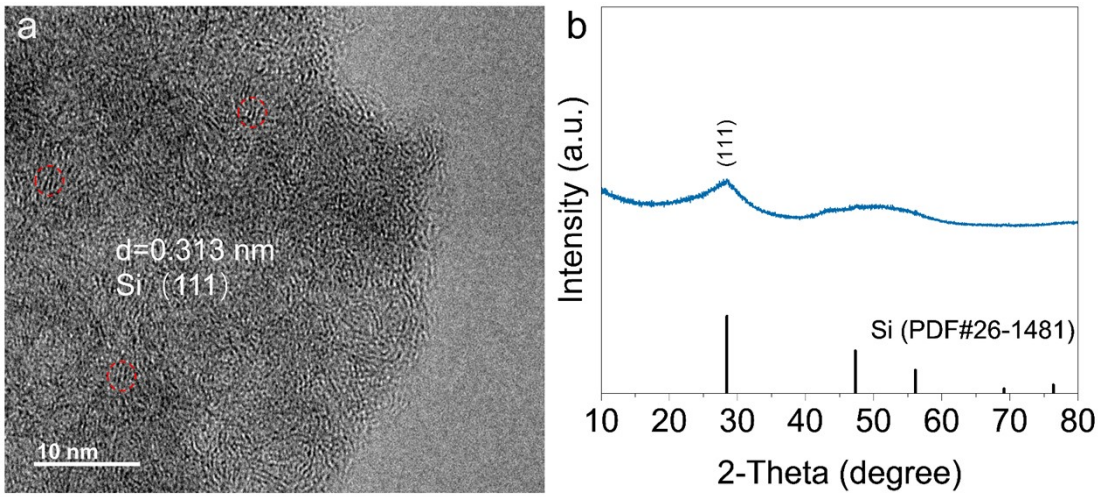

Fig. S10. (a) TEM image and (b) XRD of the commercial Si/C anode materials.

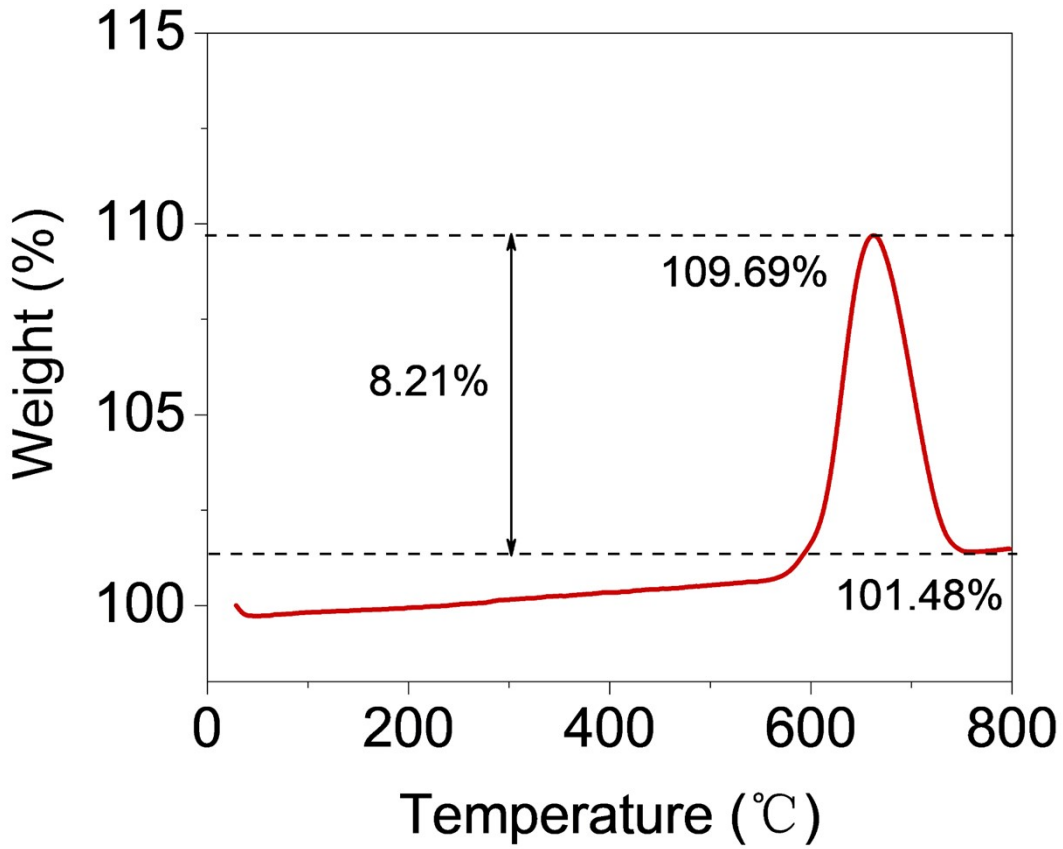

Fig. S11. The thermogravimetric curve of Si/C anode materials in O_2 atmosphere. The remaining weight of 101.48% is SiO_2 generated after oxidation. Thus, the Si content of materials is 47.4%, according to calculations.

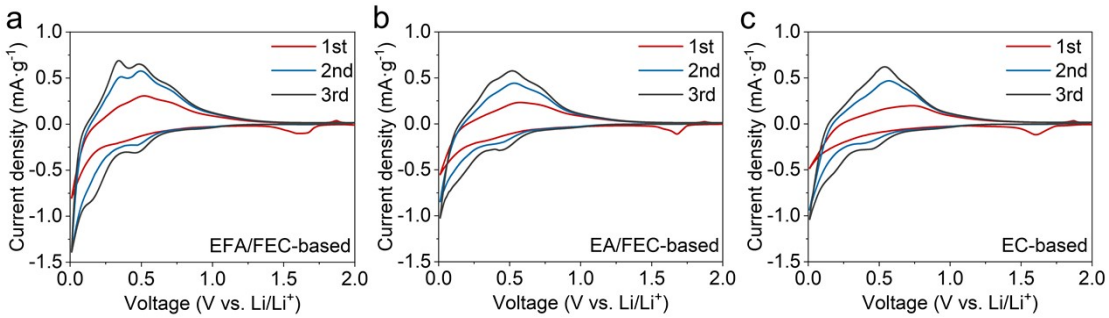

Fig. S12. The CV plots of the Si/C anodes using the (a) EFA/FEC-based electrolyte, (b) EA/FEC-based electrolyte, and (c) EC-based electrolyte.

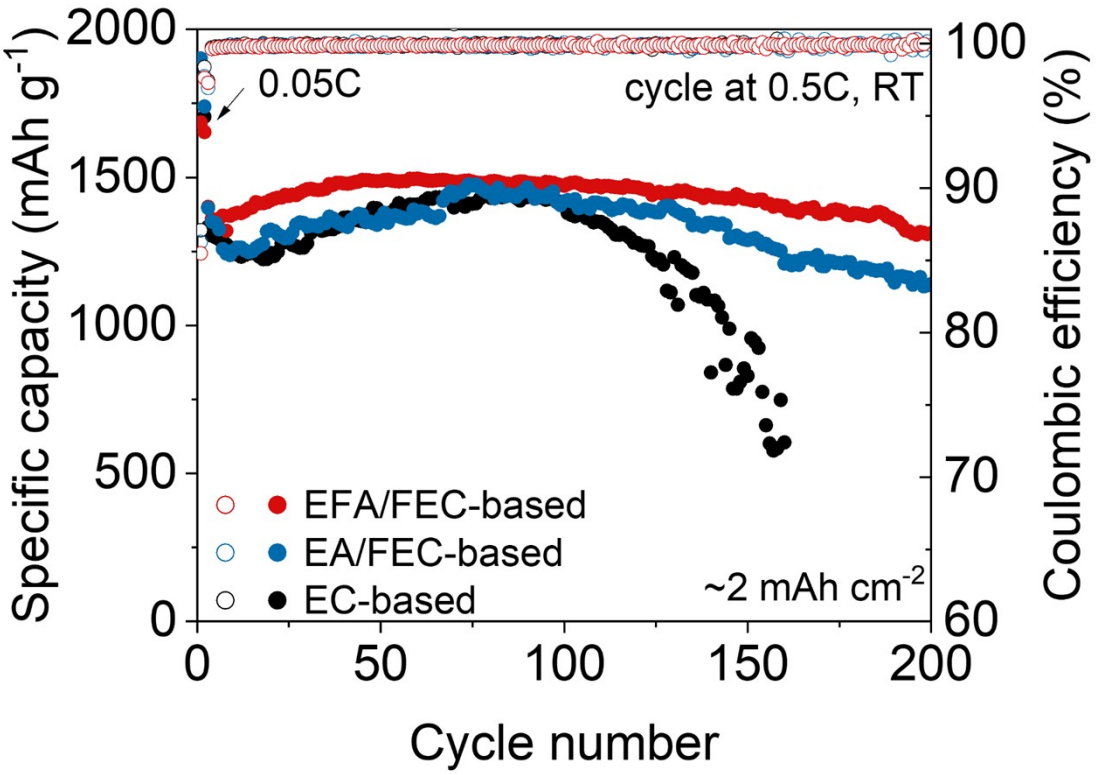

Fig. S13. The cycle performance of Li/Si cells using different electrolytes at 0.5C.

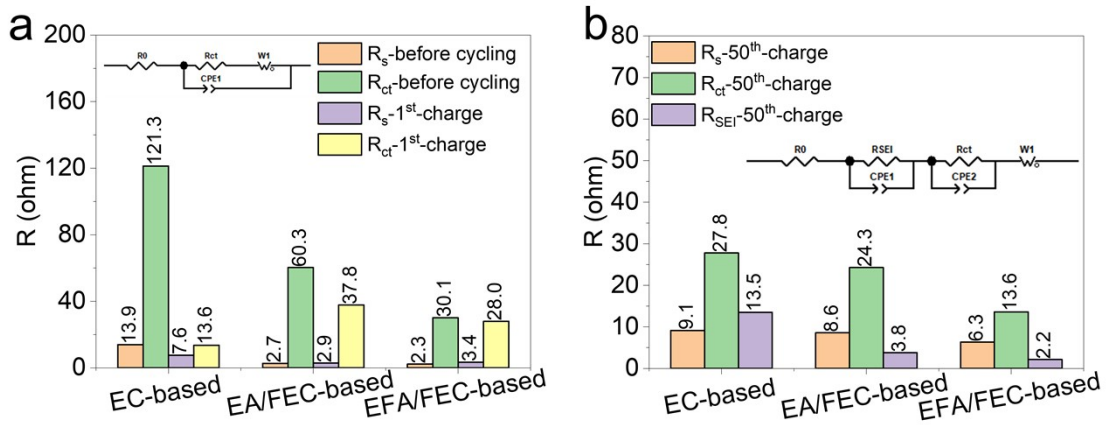

Fig. S14. The fitting results of the EIS of Li/Si cells based on the equivalent circuit (the illustration).

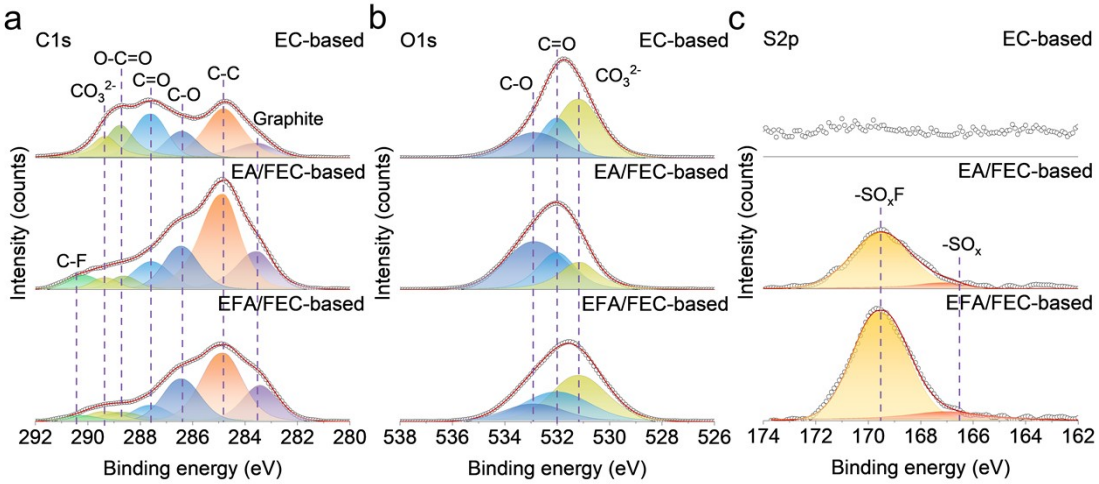

Fig. S15. The C 1s, O 1s, and S 2p XPS spectra of Si/C cathodes cycled with EC-based, EA/FEC-based, and EFA/FEC-based electrolytes.

Fig. S16. Optical image of the cross-section of the Si anodes before cycling.

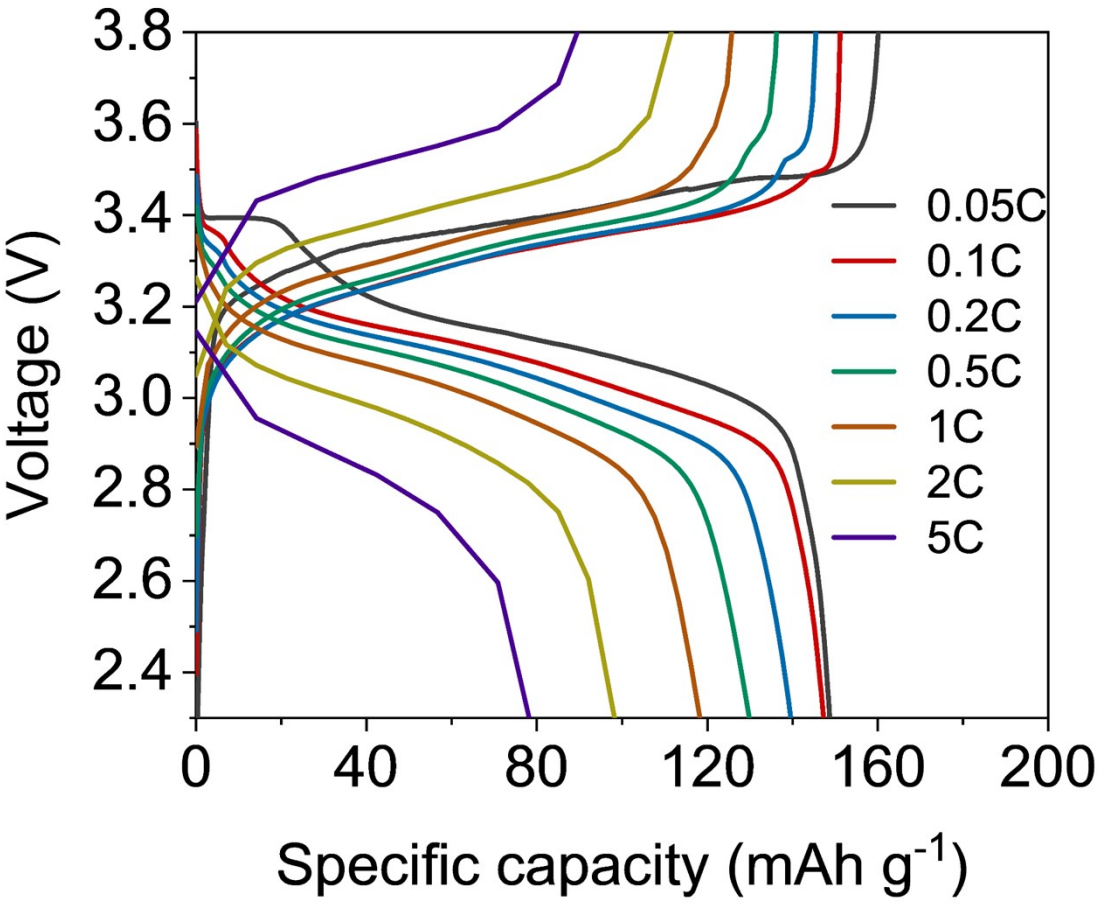

Fig. S17. The charge/discharge curves of Si/C||LFP full cell with EFA/FEC-based electrolyte at different rates.

Table S1. Corresponding calculated values for Li^+ transference number.

	$I_0(\mu A)$	$I_s(\mu A)$	$R^0(\Omega)$	$R^s(\Omega)$
EFA/FEC-based	147.30	116.10	40.03	44.32
EA/FEC-based	105.30	81.65	68.26	73.54
EC-based	29.83	17.37	310.00	408.00

Table S2. Comparisons of Li/Si cells with other published works.

electrode	Electrolyte	Capacity Retention	Ref.
nSi (7:2:1)	1 M LiFSI in FEC/BTFC/ETFA (2:2:6, by volume)	81.1% (200 cycles at 0.2C)	7
μSiO (7:1.5:1.5)	0.93 M LiFSI in TFEP/FEMC/HFE (1:3:1, by volume)	83.1% (200 cycles at 0.2C)	8
nSiO (8:1:1)	1 M LiFSI in IDE/TTE (1:3, by volume)	90% (100 cycles at 0.33C)	9
nSi (7:1.5:1.5)	5 M LiFSI in CME	83.3% (200 cycles at 0.2C)	10
nSi (7:2:1)	1.2 M LiFSI/0.05 M LiDFOB in DME/HFE/FEC (3:6:1, by volume)	87.7% (200 cycles at 0.2C)	11
μSi (6:2:2)	1 M $LiPF_6$ in FEC/SL/TTE (2:6:2, by volume)	80% (250 cycles at 0.25C)	12
SiO_x/C (7:2:1)	1 M $LiPF_6$ in EC/DEC (3:7, by volume) + 0.5 wt% APS	79.3% (200 cycles at 0.5C)	13
Si/C (8:1:1)	1 M $LiPF_6$ in EC/DEC/DMC (1:1:1, by volume) + 5 vt% TFPC	71.2% (300 cycles at 0.5C)	14
Si/C (8:1:1)	1.5 M LiFSI/0.1M LiDFOB in EFA/FEC (8:2, by volume)	88.9% (200 cycles at 0.2C) 93.7% (200 cycles at 0.5C)	**This work**

References

1 D. Van Der Spoel, E. Lindahl, B. Hess, G. Groenhof, A. E. Mark and H. J. C. Berendsen, Gromacs: Fast, Flexible, and Free, *J. Comput. Chem.*, 2005, **26**, 1701-1718.

2 M. J. Abraham, T. Murtola, R. Schulz, S. Páll, J. C. Smith, B. Hess and E. Lindahl, Gromacs: High Performance Molecular Simulations through Multi-Level Parallelism from Laptops to Supercomputers, *SoftwareX*, 2015, **1-2**, 19-25.

3 H. J. C. Berendsen, D. van der Spoel and R. van Drunen, Gromacs: A Message-Passing Parallel Molecular Dynamics Implementation, *Comput. Phys. Commun.*, 1995, **91**, 43-56.

4 Y. Duan, C. Wu, S. Chowdhury, M. C. Lee, G. Xiong, W. Zhang, R. Yang, P. Cieplak, R. Luo, T. Lee, J. Caldwell, J. Wang and P. Kollman, A Point-Charge Force Field for Molecular Mechanics Simulations of Proteins Based on Condensed-Phase Quantum Mechanical Calculations, *J. Comput. Chem.*, 2003, **24**, 1999-2012.

5 C. L. Zhao, D. X. Zhao, C. C. Bei, X. N. Meng, S. Li and Z. Z. Yang, Seven-Site Effective Pair Potential for Simulating Liquid Water, *J. Phys. Chem. B*, 2019, **123**, 4594-4603.

6 B. Hess, H. Bekker, H. J. C. Berendsen and J. G. E. M. Fraaije, Lincs: A Linear Constraint Solver for Molecular Simulations, *J. Comput. Chem.*, 1997, **18**, 1463-1472.

7 Z. Cao, X. Zheng, M. Zhou, T. Zhao, L. Lv, Y. Li, Z. Wang, W. Luo and H. Zheng, Electrolyte Solvation Engineering toward High-Rate and Low-Temperature Silicon-Based Batteries, *ACS Energy Lett.*, 2022, **7**, 3581-3592.

8 S. Yang, Y. Zhang, Z. Li, N. Takenaka, Y. Liu, H. Zou, W. Chen, M. Du, X.-J. Hong, R. Shang, E. Nakamura, Y.-P. Cai, Y.-Q. Lan, Q. Zheng, Y. Yamada and A. Yamada, Rational Electrolyte Design to Form Inorganic-Polymeric Interphase on Silicon-Based Anodes, *ACS Energy Lett.*, 2021, **6**, 1811-1820.

9 N. M. Johnson, Z. Yang, M. Kim, D.-J. Yoo, Q. Liu and Z. Zhang, Enabling Silicon Anodes with Novel Isosorbide-Based Electrolytes, *ACS Energy Lett.*, 2022, **7**, 897-905.

10 S. Mao, J. Zhang, J. Mao, Z. Shen, Z. Long, S. Zhang, Q. Wu, H. Cheng and Y. Lu, Anionic Aggregates Induced Interphase Chemistry Regulation toward Wide-Temperature Silicon-Based Batteries, *Adv. Energy Mater.*, 2024, **14**, 2401979.

11 Z. Cao, X. Zheng, Q. Qu, Y. Huang and H. Zheng, Electrolyte Design Enabling a High-Safety and High-Performance Si Anode with a Tailored Electrode-Electrolyte Interphase, *Adv. Mater.*, 2021, **33**, 2103178.

12 A. M. Li, Z. Wang, T. P. Pollard, W. Zhang, S. Tan, T. Li, C. Jayawardana, S. C. Liou, J. Rao, B. L. Lucht, E. Hu, X. Q. Yang, O. Borodin and C. Wang, High Voltage Electrolytes for Lithium-Ion Batteries with Micro-Sized Silicon Anodes, *Nat. Commun.*, 2024, **15**, 1206.

13 G. Liu, J. Gao, M. Xia, Y. Cheng, M. Wang, W. Hong, Y. Yang and J. Zheng, Strengthening the Interfacial Stability of the Silicon-Based Electrode Via an Electrolyte Additive-Allyl Phenyl Sulfone, *ACS Appl. Mater. Interfaces*, 2022, **14**, 38281-38290.

14 Z. Wen, F. Wu, L. Li, N. Chen, G. Luo, J. Du, L. Zhao, Y. Ma, Y. Li and R. Chen, Electrolyte Design Enabling Stable Solid Electrolyte Interface for High-Performance Silicon/Carbon Anodes, *ACS Appl. Mater. Interfaces*, 2022, **14**, 38807-38814.